Asian Journal of Pharmaceutical Sciences 17 (2022) 838–854

Available online at www.sciencedirect.com

ScienceDirect

journal homepage: www.elsevier.com/locate/AJPS

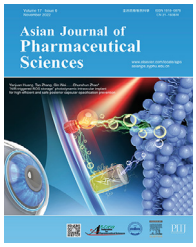

Original Research Paper

"NIR-triggered ROS storage" photodynamic intraocular implant for high-efficient and safe posterior capsular opacification prevention

Yanjuan Huang[1], *Tao Zhang*[1], *Qin Wei*[1], *Zishan Zeng*, *Yujun Gong*, *Xiaoyu Xu*, *Meixu Chen*, *Chunshun Zhao*[*]

School of Pharmaceutical Sciences, Sun Yat-sen University, Guangzhou 510006, China

ARTICLE INFO

Article history:
Received 23 March 2022
Revised 19 August 2022
Accepted 17 October 2022
Available online 5 November 2022

Keywords:
Posterior capsular opacification
Capsular tension ring
Photodynamic therapy
Endoperoxide

ABSTRACT

Posterior capsular opacification (PCO) is the leading cause of vision loss after cataract, mainly caused by the adhesion, proliferation and trans-differentiation of post-operative residual lens epithelial cells (LECs). Effective PCO prevention remains a huge challenge to ophthalmologists and researches for decades. Herein, we developed a "NIR-triggered ROS storage" intraocular implant (CTR-Py-PpIX) based on capsular tension ring (CTR), which is concurrently linked with photosensitizer protophorphyrin IX (PpIX) and energy storage 2-pyridone derivative (Py), to guarantee instantaneous and sustainable ROS generation for LECs killing, aiming to achieve more efficient and safer photodynamic therapy (PDT) to effectively prevent PCO. The silylated PpIX-Si and Py-Si were covalently conjugated to the plasma activated CTR surface to obtain CTR-Py-PpIX. Results demonstrated that CTR-Py-PpIX had dual functions of PDT and battery, in which PpIX could generate ROS extracellularly under irradiation, with one part directly inhibiting LECs by lipid peroxidation (LPO) induction of cell membranes. Meanwhile, the excess ROS stored in Py could be continuously released to amplify LPO levels after the irradiation was removed. Ultimately, the proliferation of LECs in capsular bag was completely inhibited under mild irradiation conditions, achieving a sustainable and controlled PDT effect for effective PCO prevention with good biocompatibility. This NIR-triggered ROS storage intraocular implant would provide a more efficient and safer approach for long-term PCO prevention.

[*] Corresponding author.
E-mail address: zhaocs@mail.sysu.edu.cn (C.S. Zhao).
[1] These authors contributed equally to this work.
Peer review under responsibility of Shenyang Pharmaceutical University.

https://doi.org/10.1016/j.ajps.2022.10.004

1. Introduction

Posterior capsular opacification (PCO) remains the most frequent complication after cataract surgery [1]. The rapid proliferation and migration of the residual lens epithelial cells (LECs) into posterior capsule after cataract surgery are considered as the primary mechanism of PCO [2]. This cellular behavior leads to visual axis obscuration and eventually causes a secondary vision loss [3]. According to records, the incidence of PCO is approximately 12%−67% in adults within 5 years after surgery, while it is as high as nearly 100% for children and young adults [4]. Currently, the only feasible and effective treatment for PCO clinically is Nd:YAG laser capsulotomy [5,6]. However, this procedure imposes a huge financial burden on patients and causes serious new complications [2,7,8]. Therefore, there is an urgent need to develop innovative therapeutic strategies that can effectively inhibit the proliferation or/and migration of residual LECs to prevent PCO.

To date, surgeons and researches have devoted great effort to decrease the occurrence of PCO. Many anti-proliferation drugs, including docetaxel, 5-FU, mitomycin C, etc., have been proved to inhibit the proliferation of LECs [8]. However, directly eye drops or irrigating of these non-selective drugs into the capsular bag for a few minutes were too hard to achieve effective drug concentration on the location of LECs, while poisoning normal tissues. The development of drug eluting intraocular lens (IOL) that equipped drugs via soaking in solution or surface modification, has emerged as a new promising intraocular implant drug reservoir for PCO prevention [3,9,10]. Although postoperative localized drug release is achieved, with disappointing bursts and uncontrolled drug release, satisfactory therapeutic effect has not been achieved yet. Moreover, IOL implantation may carry a postoperative risk of IOL decentration and affecting the patients' vision. Capsular tension ring (CTR), a circular and flexible poly(methyl methacrylate) (PMMA) open-loop device, has been proposed to be implanted during cataract surgery to support the capsular bag and provide long-term IOL stability when lens subluxation or zonulysis occurs [11–13]. Benefiting from not affecting the patient's vision and good biocompatibility, CTR becomes a mature tool for cataract surgeons and promising intraocular implant for PCO prevention. Our group previously developed a novel porous docetaxel loaded CTR composited by P(HEMA-co-MMA)-PMMA for long-term sustained drug release and capsule bag support [1]. Fortunately, this system realized positioning and continuous drug release for enhanced effect with attenuated toxicity. Nevertheless, due to the continuous aqueous humor circulation, the released drug would uncontrollably flow into the anterior chamber, causing unavoidable damage to the iris and cornea. It is arduous for us to bypass their severe toxicity if we applicate these potent anti-proliferation drugs. Therefore, how to improve the controllability and selectivity of PCO treatment while promising high-efficiency and low-toxicity remains a huge challenge.

Photodynamic therapy (PDT) that utilizes nontoxic photosensitizer, oxygen and harmless near infrared (NIR) light to generate cytotoxic reactive oxygen species (ROS), is a non-invasive, spatiotemporal controllable and dual-selective treatment mode [14–17]. As an effective cell-killer, PDT shows great potential in various medical diseases (*e.g.*, cancers and skin diseases) with minimized collateral damage [18–20]. Verteporfin, the first FDA-approved photosensitizer, is now becoming the most common treatment for age-related macular degeneration and neovascularization in ophthalmology [21]. Additionally, utilizing PDT to inhibit LECs proliferation has attracted great interest from researchers [4,22]. However, singlet oxygen ($^1O_2$) has an extremely short lifetime (about 10–320 ns) and diffusion distance (10–55 nm) [23], and the PDT effect would terminate immediately once removing irradiation, causing a large amount of $^1O_2$ to be wasted before damaging cells, which compromises the PDT effect. Although prolonging light duration or increasing light power to generate robust $^1O_2$ can sustain the PDT effect, possible side effects such as retinal damage and tissue hypoxia may occur. Therefore, it was envisaged that the excess $^1O_2$ produced by PDT could be temporarily stored to reduce energy loss, and then continuously released when removing light, a more efficient and safer long-term PDT would be achieved.

Based on the above issues, herein, we developed a "NIR-triggered ROS storage" CTR intraocular implantation system (CTR-Py-PpIX), which simultaneously functionalized with PDT trigger and ROS reservoir to induce instantaneous and sustainable $^1O_2$ generation, aiming to achieve localized long-term effective PCO prevention. Protophorphyrin IX (PpIX), a clinically commonly used photosensitizer, was selected as the ROS generator. 2-pyridone derivative (Py) that can capture $^1O_2$ to form 2-pyridone endoperoxide and release $^1O_2$ efficiently at mild human temperature, was chosen for ROS storage [24,25]. Firstly, the photosensitizer unit PpIX and energy storage unit Py were silylated to synthesize PpIX-Si and Py-Si. Next, the inert PMMA CTR was activated by plasma to produce reactive hydroxyl groups in its surface. Then, PpIX-Si and Py-Si were covalently linked to the activated CTR surface via silanization to obtain the "NIR-triggered ROS storage" CTR implant CTR-Py-PpIX (Scheme 1A). After implanting CTR-Py-PpIX into the lens capsular bag (Scheme 1B), PpIX could generate ROS extracellularly under mild NIR conditions, with one part immediately eliminating the proliferative LECs in the equatorial region by cell membranes lipid peroxidation (LPO) induction, enabling spatiotemporally controllable PDT effect. After the NIR irradiation was removed, the excess $^1O_2$ stored in Py during the PDT process was continuously released to damage the cell membrane, aggravating LPO levels to exacerbate cell death. With instantaneous and sustainable $^1O_2$ release during and after short-time irradiation, the proliferation of LECs was completely inhibited, realizing a more effective PCO prevention with good biocompatibility.

Compared with previous works, this concept of CTR design represents the following advantages: (1) Localized killing of LECs without affecting the visual axis. (2) Covalent linking of functional monomers to maintain long-term stability but avoid potential toxicity. (3) Dual function of PDT and battery ensures instantaneous and sustainable ROS for long-term efficient and safer PDT. The proposed "NIR-triggered ROS storage" intraocular implant provides a more efficient and safer approach for preventing PCO.

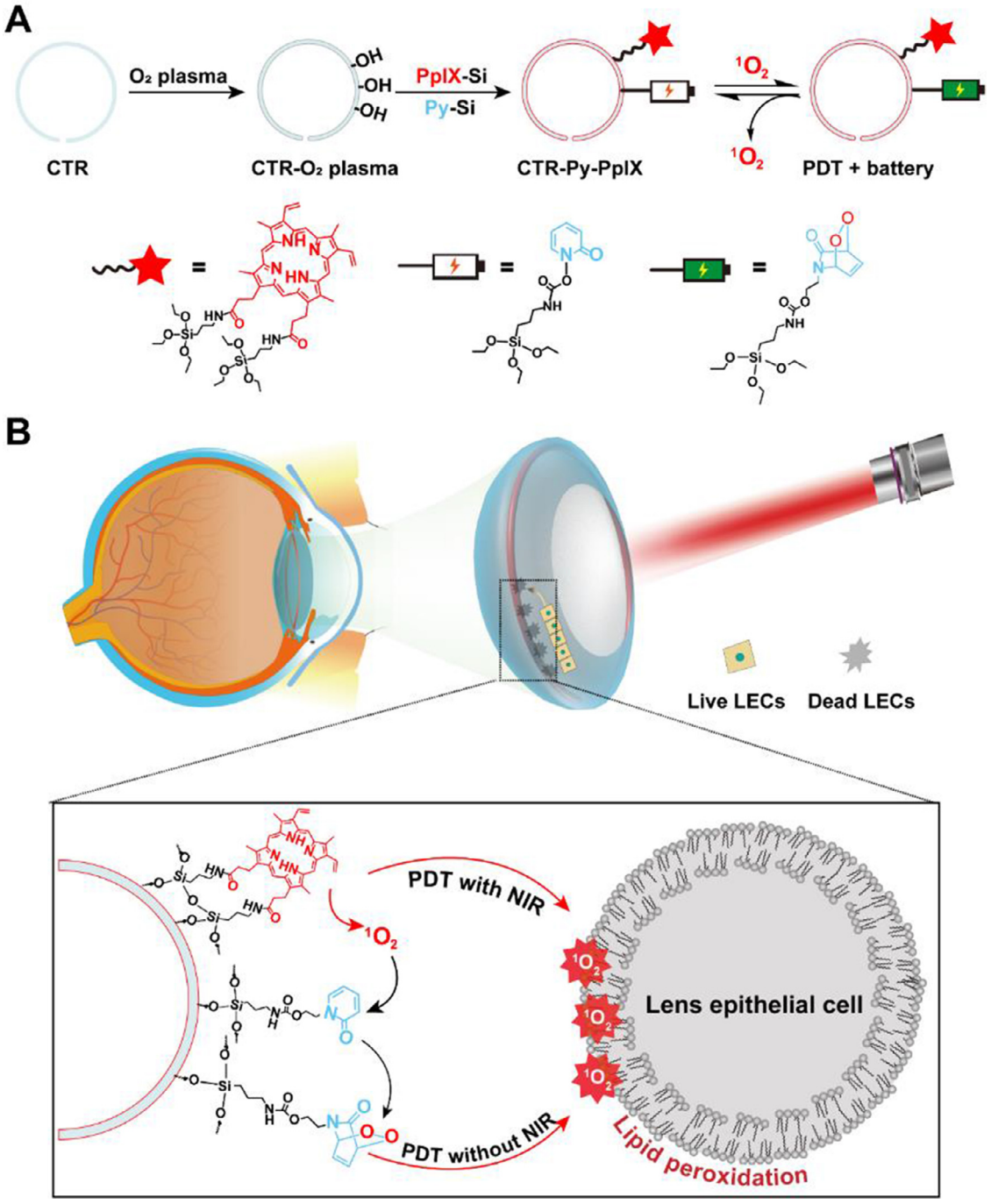

Scheme 1 – Schematic illustration of (A) the preparation of CTR-Py-PpIX and (B) the inhibition of PCO. The CTR-Py-PpIX implanted in the capsule inhibits the LECs by instantaneous and sustainable $^1O_2$ generation.

2. Materials and methods

2.1. *Materials, cell lines and animals*

Protoporphyrin IX (PpIX) was purchased from Howei Chemical Co., Ltd. (Guangzhou, China). 2-hydroxypyridine was purchased from Macklin Biochemical Co., Ltd. (Shanghai, China). Methyl methacrylate (MMA), 2-bromine ethanol, 3-aminopropyl triethoxysilane (APTES), 1-ethyl-3-(3-dimethylaminopropyl)carbodiimide·hydrochloride (EDC·HCl), 3-isocyanatopropyltriethoxysilane (IPTS), ethylene glycol dimethacrylate (EGDMA), 1,3-diphenylisobenzofuran (DPBF), fluorescein diacetate (FDA) and azodiisobutyronitrile (AIBN) were obtained from Aladdin Reagents Co., Ltd. (Shanghai, China). 4-dimethylaminopyridine (DMAP) was obtained from Bide Pharmatech Co., Ltd. (Shanghai, China). N, N-diisopropyl ethylamine (DIPEA) was purchased from Beijing Ouhe Technology Co., Ltd. (Beijing, China). Singlet Oxygen Sensor Green probe (SOSG) and BODIPY-C11 were purchased

from Thermo Fisher Scientific Inc. (Waltham, MA, USA). Propidium iodide (PI), trypsin, 2′,7′-dichlorofluorescein diacetate (DCFH-DA), 3-(4,5-dimethyl-2-thiazolyl)−2,5-diphenyl-2-H-tetrazolium bromide (MTT) and 4′, 6-diamidino-2-phenylindole (DAPI) were purchased from Sigma-Aldrich (St. Louis, USA). All other solvents and reagents were directly used as analytical pure without further purification.

Human lens epithelium cell lines (HLECs) and mouse L929 fibroblastic cell lines were purchased from the Laboratory Animal Center of Sun Yat-sen University (Guangzhou, China). Cells were cultured in Dulbecco's Modified Eagle Medium (DMEM, Gibco) containing 10% fetal bovine serum (FBS, Gibico) and 1% antibiotics (Sigma-Aldrich) in a humidified incubator with 5% CO_2 and 95% air at 37 °C.

New Zealand White rabbits (1.8–2 kg) were obtained from the Laboratory Animal Center of Sun Yat-sen University (Guangzhou, China). All animal experiments were conducted under the regulations approved by the Institutional Animal Care and Use Committee of Sun Yat-sen University.

2.2. Synthesis of functional monomers Py-Si and PpIX-Si

2-hydroxypyridine (714 mg), 2-bromoethanol (625 mg) and potassium carbonate (1.04 g) were dissolved in 20 ml DMF and stirred at 65 °C overnight. The intermediate Py-OH was purified by silica gel column chromatography (petroleum ether: ethyl acetate = 1:1, v/v). ^{1}H NMR (400 MHz, AVANCE-400, Bruker, Germany): δ 7.41–7.36 (m, 2H, NCHCH, COCHCH), 6.59 (d, J = 9.0 Hz, 1H, COCHCH), 6.27–6.19 (m, 1H, NCHCH), 4.12 (t, J = 5.0 Hz, 2H, NCH_2CH_2), 3.93 (t, J = 5.0 Hz, 2H, NCH_2CH_2).

Next, Py-OH (139 mg) was dissolved in CH_2Cl_2, then 192 µl IPTS and 209 µl DIPEA were added, and the reaction was stirred and refluxed for 18 h at 40 °C under N_2 atmosphere. After that, the final product Py-Si was purified by silica gel column chromatography (CH_2Cl_2: methanol = 1:10, v/v). The successful synthesis of Py-Si was confirmed by ^{1}H NMR and ESI-MS (LCQ DECA XP, Thermo). ^{1}H NMR (400 MHz, $CDCl_3$): δ 7.34 (t, J = 9.1 Hz,1H, COCHCH), 7.26 (d, J = 6.8, 1H, NCHCH), 6.58 (d, J = 9.1 Hz, 1H, COCHCH), 6.16 (t, J = 6.8, 1H, NCHCH), 5.07 (s, 1H,CONH), 4.37 (t, J = 5.4 Hz, 2H, NCH_2CH_2), 4.19 (t, J = 5.4 Hz, 2H, NCH_2CH_2), 3.83 (q, J = 7.0 Hz, 6H, OCH_2CH_3), 3.18 (m, 2H, $NHCH_2CH_2$), 1.63 (t, J = 7.3 Hz, 2H, NCH_2CH_2), 1.23 (t, J = 7.0 Hz, 9H, OCH_2CH_3), 0.73–0.53 (m, 2H, $CH_2CH_2CH_2$). ESI-MS for $C_{17}H_{30}N_2O_6Si$: m/z $[M+H]^+$ calcd: 387.19, found: 387.28.

To synthesis PpIX-Si, PpIX (0.01 mmol) was dissolved in 5 ml DMF, then EDC·HCl (0.10 mmol) and DMAP (0.08 mmol) were added. The mixture was stirred for 1 h at room temperature under N_2 atmosphere in the dark, then APTES (0.20 mmol) was rapidly injected into the above reaction, and the mixture was continuously stirred at room temperature under dark for 12 h. After that, the product was added dropwise to 10 ml cold ether solution and centrifuged (1000 rpm) at 4 °C for 15 min, then the supernatant was removed and the residual ether was evaporated, the obtained PpIX-Si was stored in methanol for further use. The successful synthesis of PpIX-Si was characterized by Fourier transform infrared (FTIR) spectroscopy (VERTEX 70, Bruker, Germany) and ESI-MS. ESI-MS for $C_{52}H_{76}N_6O_8Si_2$: m/z $[M+H]^+$ calcd: 968.53, found: 969.55.

2.3. $^1O_2$ generation detection

The NIR-triggered $^1O_2$ generation capacity of PpIX-Si was measured using DPBF as an $^1O_2$ indicator, which can efficiently trap $^1O_2$ and induce a drop in absorbance at 412 nm [26]. Typically, 500 µl PpIX-Si (100 µM) methanol solution was added into 2 ml of DPBF (60 µM) solution. The mixture was irradiated with a laser (630 nm, 100 mW/cm^2) for 1 min, and the UV–Vis absorption spectra was recorded immediately by a UV–vis spectrophotometer (UV2600, Techcomp, China). The procedure was repeated for 6 times. Blank DPBF solution was set as control. The degradation rate of DPBF (%) was calculated as A_t/A_0, where A_0 represents the absorbance at 412 nm in 0 min, and A_t represents the absorbance at other detected time points.

2.4. $^1O_2$ capture and release capacity of Py-Si

Firstly, the optimal molar ratio of PpIX-Si and Py-Si for $^1O_2$ capture and release ability of Py-Si was investigated. Briefly, PpIX-Si (100 µM) was mixed with 1 mM (molar ratio PpIX-Si/Py-Si = 1/10), 5 mM (PpIX-Si/Py-Si = 1/50) and 10 mM (PpIX-Si/Py-Si = 1/100) of Py-Si in methanol solution respectively, then the mixtures were irradiated with a 630 nm laser (100 mW/cm^2) for 5 min. After that, 2 ml DPBF (60 µM) solution was added to each mixture, and the UV–vis absorbance changes at different times were monitored by UV–vis spectroscopy.

Next, the $^1O_2$ release ability of Py-Si at the optimized molar ratio (PpIX-Si/Py-Si = 1/50) was further investigated. Typically, PpIX-Si (100 µM) was mixed with 5 mM of Py-Si (PpIX-Si/Py-Si = 1/50) in methanol solution, then the mixture was irradiated with a 630 nm laser (100 mW/cm^2) for 5 min. After that, 2 ml DPBF (60 µM) solution was added and the mixture was incubated at 37 °C for different times. Blank DPBF solution, PpIX-Si (100 µM) and Py-Si (5 mM) were set as controls. The UV–Vis absorbance change of each solution was monitored by UV–vis spectroscopy.

2.5. Preparation of the surface functionalized CTR (CTR-Py-PpIX)

2.5.1. Preparation of PMMA

EGDMA crosslinker (200 µl) and AIBN initiator (100 mg) were mixed with 10 ml MMA monomer solution, then pre-polymerized in a 37 °C water bath for 30 min. After that, the mixture was poured into a mold and placed in a 60 °C oven for 4 h to synthesize PMMA polymer. The obtained PMMA polymer was placed in a Soxhlet extractor and refluxed with methanol for 24 h to remove the unreacted monomers and initiators, and then dried at room temperature.

2.5.2. Preparation of CTR

The obtained PMMA sheet was cut into blocks of about 13 mm × 13 mm, and then an electric sander was applied to grind it into a bottom-opened ring-shaped tension ring with an outer diameter of about 11.5 mm and an inner diameter of about 11 mm and washed for subsequently studies. The PMMA sheet was polished into a 14 mm diameter

Table 1 – Feeding concentration of CTR-Py-PpIX, CTR-PpIX and CTR-Py.

Sample	PpIX-Si (mM)	Py-Si (mM)
CTR-Py-PpIX-1	0.5	25
CTR-Py-PpIX-2	0.2	10
CTR-Py-PpIX-3	0.08	4
CTR-Py-PpIX-4	0.025	1.25
CTR-Py-PpIX-5	0.01	0.5
CTR-Py	0	10
CTR-PpIX	0.2	0

disk and a 5 mm × 5 mm square sheet for use by a similar way.

2.5.3. *Preparation of CTR-O_2 plasma*

Briefly, the polished CTR was sequentially washed with surfactant and 95% ethanol in an ultrasonic cleaner for 5 min respectively, and then dried in an oven at 50 °C. The cleaned CTR was delivered to the inductively coupled plasma etching system (iCAP6500Duo, ThermoFisher), after evacuation, O_2 was introduced into the chamber and transformed into O_2 plasma under high-pressure ionization. The treatment was carried out for 5 min, and the other side of CTR was activated by the same method to obtain CTR-O_2 plasma.

2.5.4. *Preparation of CTR-Py-PpIX*

The photosensitizer unit PpIX-Si and the energy storage unit Py-Si were covalently conjugated on the CTR surface, because the silylation reagent can react efficiently and quickly with the hydroxyl group on CTR. To investigate the feeding concentration of PpIX-Si and Py-Si on grafting degree, the feeding concentration (mM) of $C_{(PpIX\text{-}Si)}/C_{(Py\text{-}Si)}$ in methanol was fixed at 1:50, and series concentrations of PpIX-Si/Py-Si (0.01/0.5, 0.025/1.25, 0.08/4, 0.2/10, 0.5/25 mM) to prepare CTR-Py-PpIX were conducted (Table 1). Each experimental group was mixed with 1% ammonia solution to a total volume of 4 ml, then CTR-O_2 plasma was immediately immersed into the ammonia solution and shaken for 12 h. Then it was put into a 60 °C oven and cure for 12 h, and finally washed with a large amount of water and ethanol to obtain the CTR with different surface modifications. CTR-Py and CTR-PpIX were prepared in the same way, meanwhile, PMMA wafers and PMMA squares were also treated in the same way.

2.6. *Characterization of CTR-Py-PpIX*

The surface morphology and atomic composition of CTR, CTR-O_2 plasma, CTR-Py, CTR-PpIX and CTR-Py-PpIX were observed by thermal field emission scanning electron microscope (SEM-EDS) (Quanta 400F, FEI, USA) and X-ray photoelectron spectroscopy (XPS) (Thermo Fisher Scientific, ESCALAB 250), respectively. The structure of CTR, CTR-Py, CTR-PpIX and CTR-Py-PpIX were verified by FTIR. The intrinsic water wettability of PMMA, PMMA-O_2 plasma, PMMA-Py, PMMA-PpIX and PMMA-Py-PpIX were detected by Contact Angle Measurements (DCAT21, Dataphy Instruments, Germany) using the william plate method. The physicochemical properties of CTR, including the surface quality, size, mechanical properties were investigated based on the regulation in the "Pharmaceutical Industry Standard of the People's Republic of China (2017 Edition)" on the CTR in ophthalmic optics. To detect the content of Si, CTR-Py-PpIX was digested with aqua regia for 24 h, then the sample was dried and re-dissolved in 8 ml nitric acid solution (4%, v/v), finally detected by Inductively Coupled Plasma-Atomic Emission Spectrometry (ICP-AES, Optima 8300, Perkin–Elmer).

2.7. *Anti-cell adhesion and proliferation assay*

PMMA discs of CTR, CTR-Py, CTR-PpIX and CTR-Py-PpIX with diameters of 14 mm were placed in 24-well plates, then HLECs were seeded in 24-well plates (5×10^4 cells/well). After incubated for 24 h under dark, cells were carefully washed, and 500 μl (5 μg/ml) of FDA solution was added to each well, and the cell adhesion and proliferation in PMMA of different groups were observed under an inverted fluorescence microscope (IX73, Olympus, Japan).

2.8. *$^1O_2$ capture and release capacity of CTR-Py-PpIX*

A water-soluble $^1O_2$ probe SOSG was used to investigate the $^1O_2$ capture and release capacity of CTR-Py-PpIX. CTR-Py-PpIX was placed in a fluorescent cuvette, then 2 ml SOSG aqueous solution (5 μM) was added, followed by irradiating under an LED lamp (630 nm, 20 mW/cm²) for 5 min. After the illumination, the fluorescence intensity of the mixture was immediately determined by a fluorescence spectrometer (Fluoromax-4, HORIBA, USA, Ex = 488 nm, Em = 520 nm). The measurement was performed every 5 min for a total of 30 min under dark. Subsequently, the SOSG solution was removed and 2 ml fresh SOSG aqueous solution (5 μM) was added, then the mixture was irradiated and detected according to the above procedure. The operation was repeated for 3 times, and the fluorescence changes of SOSG during the 3 cycles were calculated.

2.9. *In vitro stability of CTR-Py-PpIX*

To investigate the *in vitro* stability in physiological environment, CTR-Py-PpIX was immersed in 3 ml artificial tears (0.1% sodium hyaluronate) with stirring at 37 °C in a shaker, 300 μl sample was taken out at scheduled time points (1, 2, 4, 8 and 16 d) and replaced with an equal volume of artificial tears. The samples were re-dissolved in 4% HNO_3, and the contents of Si were detected by ICP-AES.

To investigate whether the PDT efficiency would be retained after implantation, the CTR-Py-PpIX which immersed in 3 ml artificial tears for 1 and 16 d were taken out, and its $^1O_2$ capture and release capacity was evaluated according to the procedures detailed in Section 2.7.

2.10. *Treatment procedures of CTR for cell experiments*

CTR with different surface modifications were sterilized under UV light for 30 min, and then fully immersed in DMEM. In all the *in vitro* cell experiments, the CTR were carefully transferred to the cell plate with tweezers and lightly covered

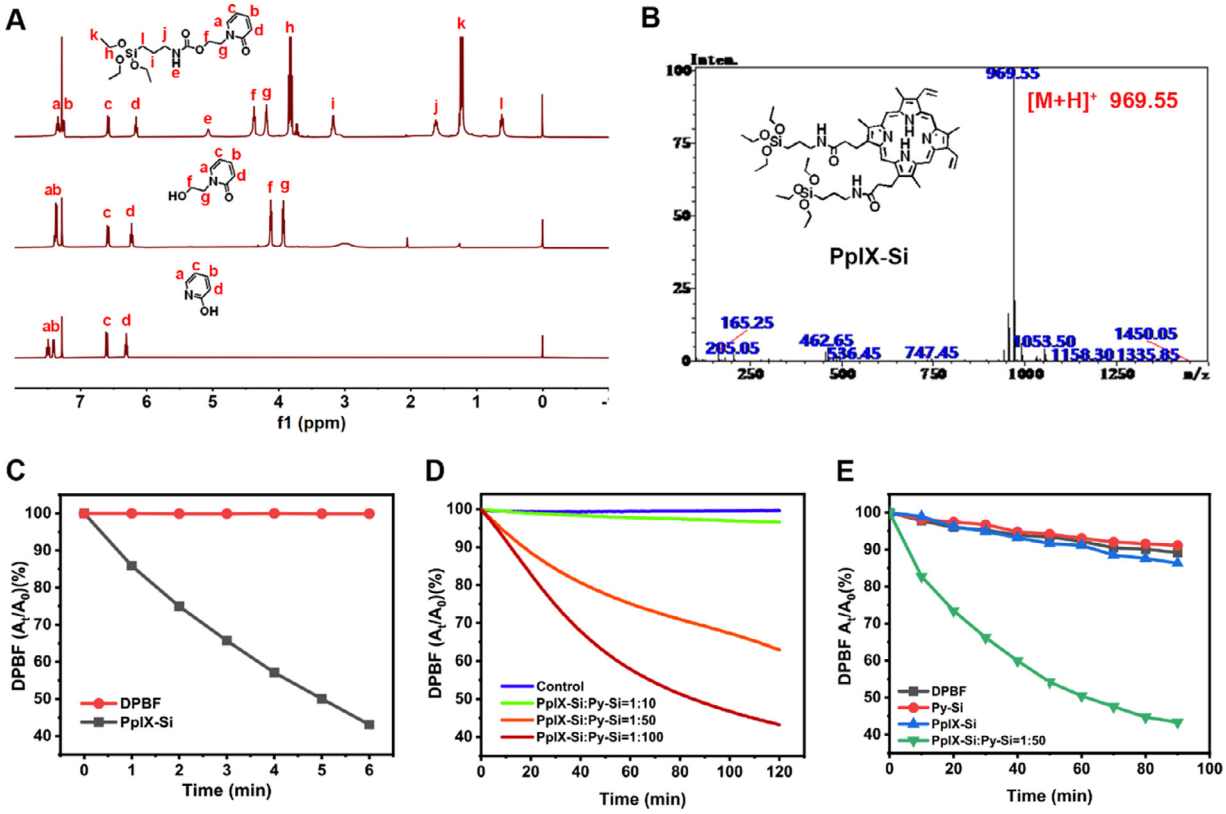

Fig. 1 – (A) The ^{1}H NMR spectra of Py-OH and Py-Si in $CDCl_3$. (B) The ESI-MS spectra of PpIX-Si. (C) The $^1O_2$ generation of PpIX-Si under different laser irradiation (630 nm, 100 mW cm^{-2}) times. (D) The $^1O_2$ generation of pre-irradiated (630 nm, 100 mW/cm^2, 5 min) PpIX-Si/Py-Si mixture with different concentration ratio. (E) The degradation rate of DPBF with pre-irradiation of different solution for 5 min.

on the cells to ensure it did not float on the culture medium. At the meanwhile, the cell culture plates kept relatively static to prevent mechanical damage.

2.11. *In vitro cytotoxicity of CTR-Py-PpIX*

The *in vitro* cytotoxicity of CTR with or without $^1O_2$ storage were directly visualized by live/dead cell staining assay. Briefly, HLECs were seeded in 24-well plates (1×10^5 cells/well) and incubated overnight. To investigate the cytotoxicity of CTR without $^1O_2$ storage, CTR, CTR-Py, CTR-PpIX and CTR-Py-PpIX were lightly covered on the cells. After that, cells were irradiated or not with 630 nm NIR light at a laser power of 100 or 200 mW/cm^2 for 5 or 10 min, respectively. Cells were then incubated for an additional 3 h, then the CTR was taken out before the cells were stained with FDA and PI co-staining buffer, followed by observation with a fluorescence microscope. To investigate the cytotoxicity of CTR with $^1O_2$ storage, CTR, CTR-Py, CTR-PpIX and CTR-Py-PpIX were pre-illuminated with 630 nm laser (100 mW/cm^2) for 5 min, and then immediately covered on the cell surface. After 3 h of incubation, the CTRs were taken out, and cells were stained with FDA and PI co-staining buffer, and then imaged by fluorescence microscope.

2.12. *Intracellular ROS and LPO levels detection*

Intracellular ROS and LPO levels were detected by confocal laser scanning microscopy (CLSM) (LSM 710, Zeiss, Germany) using DCFH-DA and Bodipy C11 as detection indicators, respectively. Typically, HLECs were seeded on glass coverslips in 24-well plates and incubated overnight. The cell medium was replaced by DMEM containing DCFH-DA (10 μM) or Bodipy C11 (10 μM), respectively, and incubated for 30 min, then cells were washed with PBS for three times.

For the evaluation of ROS generation and LPO levels of CTR without $^1O_2$ storage, CTR, CTR-Py, CTR-PpIX and CTR-Py-PpIX were lightly covered on the DCFH-DA or Bodipy C11 treated cells respectively, then they were exposed to 630 nm laser (100 mW/cm^2) for 5 min. After incubated for an additional 1.5 h, the CTR was taken out and the cells were washed, fixed with 4% paraformaldehyde, then stained with DAPI and directly imaged by CLSM. Free PpIX-Si which pre-illuminated with 630 nm laser (100 mW/cm^2, 5 min) before incubated with cells for 1.5 h was set as positive control. To investigate the ROS generation and LPO levels of CTR with $^1O_2$ storage, CTR, CTR-Py, CTR-PpIX and CTR-Py-PpIX were pre-irradiated with 630 nm laser (100 mW/cm^2) for 5 min, and then immediately covered on the surface of the DCFH-DA or

Bodipy C11 treated cells and incubated for 10 min, 30 min, 1 h and 1.5 h, respectively. After that, the CTR was taken out, and the cells were washed, fixed, stained with DAPI and directly visualized by CLSM. PpIX-Si (1 μM) + Py-Si which pre-illuminated with 630 nm laser (100 mW/cm², 5 min) before incubated with cells for 1.5 h was set as positive control. In addition, the ROS generation of photosensitizer unit and energy storage unit were also detected. Briefly, PpIX-Si (1 μM), Py-Si (50 μM) and PpIX-Si + Py-Si were pre-irradiated with 630 nm laser (100 mW/cm²) for 5 min, then PpIX-Si and Py-Si were incubated with the DCFH-DA-treated cells for 1.5 h, and PpIX-Si + Py-Si was incubated with the DCFH-DA-treated cells for 10 min, 30 min, 1 h and 1.5 h, respectively. After that, the cells were washed, fixed, stained with DAPI and directly imaged by CLSM.

2.13. *Pharmacodynamics investigation in the isolated lens capsular bag*

2.13.1. *Gain and culture of lens capsular bag*

The isolation and culture of the lens capsular bag were conducted according to our previously reported method [1]. New Zealand rabbits were sacrificed, then the eyeballs were quickly and carefully isolated using tweezers and surgical scissors and immediately soaked in fresh pre-cooled PBS solution containing 5% double antibody. After soaking in 75% ethanol for 30–60 s, the eyeballs were transferred into clean workbench, then washed 3 times with PBS containing 5% double antibody, and soaked them for later use. The extraction was performed under a dissecting microscope and the procedures were detailed as follows. Firstly, the eyeballs were fixed, the cornea and iris along the edge of the cornea and sclera were cut off using tissue scissors. After the lens were isolated, the remaining vitreous attached to the back of the lens was cut and peeled off. Next, the capsulotomy needle was applied to cut the anterior lens capsule under the dissecting microscope, and the PBS solution was injected close to the cut anterior capsule with a syringe to separate the lens capsular bag from the lens cortex using water separation. Finally, the lens nucleus were cut with ophthalmic scissors, the lens cortex and nucleus were taken out, and the residual cortex and nucleus were completely removed by rinsing with PBS. The isolated capsular bags were transferred to a 24-well plate and maintained in a cell incubator.

2.13.2. *PDT therapeutic effect of CTR*

To investigate the therapeutic effect of PDT, CTR, CTR-Py, CTR-PpIX (low power group, high power group and long irradiation time group) and CTR-Py-PpIX were carefully implanted into the lens capsular bag. The culture medium of control group was replaced by 1 ml of fresh culture medium at 1 d, 3 d, 5 d and 7 d of incubation without any other operations. The capsular bag in CTR, CTR-Py and CTR-Py-PpIX groups were irradiated with 630 nm laser (100 mW/cm²) for 5 min at Day 1, 3 and 5. After incubated for an additional 2 h, the capsular bag was washed and 1 ml of fresh culture medium was added. At Day 7 of culture, the culture medium was replaced again with 1 ml of fresh medium. For CTR-PpIX, low power (100 mW/cm²) and short irradiation time (5 min) group, high power (200 mW/cm²) and short irradiation time group and low power and long irradiation time (10 min) group were defined as CTR-PpIX (LS), CTR-PpIX (HS) and CTR-PpIX (LL), respectively. They were received the same treatment regimen to that of CTR-Py-PpIX group except for different irradiation conditions. The proliferation of the residual LECs on the capsular bag was photographed under a digital inverted microscope at 1, 3, 5 and 7 d after fresh medium was replaced.

2.14. *Toxicity of CTR-Py-PpIX*

Cell morphology observation and MTT assay were conducted to evaluate whether the biocompatibility of CTR-Py-PpIX is suitable for biomedical application. The CTR-Py-PpIX was sterilized under UV light for 30 min, and then the DMEM medium containing 10% FBS was added at a final concentration of 0.2 g/ml. After leaching in a 37 °C incubator for 24 h, the culture medium was filtered through a 0.22 μm filter for subsequent use. L929 cells seeded on 96-well plates (5×10^3 cells/well) were treated with 200 μl fresh cell culture medium, leaching solution of CTR-Py-PpIX and 0.64% of phenol solution (positive control) and incubation for 48 h. The cell morphology was imaged and the cell viability was detected by MTT assay.

2.15. *Statistical analysis*

Data were expressed as mean ± standard deviation (SD). Statistical differences between groups were determined by ordinary one-way ANOVA using Graphpad Prism 8.3.0 (GraphPad software, CA, USA). Statistical significance was considered when a value of $P < 0.05$ ($^{*}P < 0.05$, $^{**}P < 0.01$, $^{***}P < 0.001$).

3. Results and discussion

3.1. *Synthesis and characterization of functional monomers Py-Si and PpIX-Si*

The detailed synthetic route of energy storage monomer Py-Si was displayed in Fig. S1. Firstly, 2-hydroxypyridine was reacted with 2-bromoethanol to synthesis Py-OH. Then, Py-OH was further reacted with IPTS to synthesis Py-Si. The successful synthesis of Py-OH was verified by ^{1}H NMR (Fig. 1**A**) and the structure of Py-Si was confirmed by ^{1}H NMR (Fig. 1A) and ESI-MS (Fig. S2). Photosensitizer monomer PpIX-Si was synthesized by reacting PpIX with APTES via amide reaction between the carboxyl group of PpIX and the amino group of APTES (Fig. S3). The successful synthesis of PpIX-Si was confirmed by FTIR and ESI-MS. Compared with the FTIR spectrum of PpIX, the stretching vibration of the carboxyl group (C = O) of PpIX at 1706 cm^{-1} was blue-shifted to 1637 cm^{-1} with a weaker absorption after conjugating with APTES, indicating the successful formation of amide bond in PpIX-Si. Particularly, a new stretching vibration peak was observed at 1001 cm^{-1}, which was assigned to the characteristic C-Si-O bond, suggesting that APTES has been successfully linked to PpIX (Fig. S4). Moreover, the ESI-MS spectrum of PpIX-Si (m/z, $[M+H]^+$, 969.55) exhibited in Fig. 1B verified that both carboxyl groups of PpIX were grafted with APTES.

3.2. *Functional characterization of PpIX-Si and Py-Si*

3.2.1. *$^1O_2$ generation capacity of PpIX-Si*

The $^1O_2$ generation capacity of PpIX-Si under irradiation was examined using DPBF as the $^1O_2$ indicator. A sharp absorbance decrease was observed in PpIX-Si group, and the degradation rate of DPBF reached 50% after 5 min of illumination, indicating that PpIX-Si had a good $^1O_2$ generation capacity, laying a strong foundation for its application as a $^1O_2$ donor (Fig. 1C).

3.2.2. *$^1O_2$ capture and release capacity of Py-Si*

Since Py-Si was designed to serve as a $^1O_2$ reservoir, the $^1O_2$ capture and release capacity was investigated using DPBF as an indicator. To screen the optimal molar ratio of PpIX-Si/Py-Si for better $^1O_2$ capture and release, certain amount of PpIX-Si was mixed with Py-Si at different molar ratios (PpIX-Si:Py-Si = 1:10, 1:50 and 1:100). After irradiation for 5 min, DPBF was added and its absorption was recorded at scheduled time points for 2 h (Fig. 1D). In the presence of PpIX-Si, the degradation rate of DPBF increased with the increasing ratio of Py-Si. When PpIX-Si:Py-Si was 1:10, DPBF degraded slightly during 2 h period, when its ratio increased to 1:50, the DPBF degradation rate increased significantly, and when its ratio reached to 1:100, the DPBF degradation rate further increased, which degraded to 49% at 90 min. The result suggested that the $^1O_2$ generated by PpIX-Si could be temporarily stored by Py-Si and then gradually released, and the release rate of $^1O_2$ increased with the ratio of Py-Si increased, revealing the excellent capacity of Py-Si as $^1O_2$ reservoir. Considering that the constructed intraocular implant needs to produce instantaneous $^1O_2$ and long-term $^1O_2$ release, the molar ratio of PpIX-Si:Py-Si = 1:50 was chosen for subsequent study.

Next, we further determined the $^1O_2$ storage and release capacity of Py-Si at 37 °C with the optimized molar ratio (PpIX-Si/Py-Si = 1/50) to investigate whether Py-Si could release the stored $^1O_2$ at body temperature. The blank DPBF group had a slight degradation (11.8%) after 90 min of incubation, possibly due to the thermal-induced decomposition of DPBF (Fig. 1E). By contrast, the pre-illuminated Py-Si group observed no obvious degradation, indicating that Py-Si cannot generate $^1O_2$ before and after illumination. Moreover, no significant degradation of DPBF was detected in the pre-irradiated PpIX-Si group either, which might be due to the short half-life and limited diffusion radius of $^1O_2$ generated by PpIX-Si [27], making the $^1O_2$ generation stop immediately after the cessation of illumination. In sharp contrast, the pre-illuminated PpIX/Py-Si mixed group displayed remarkable degradation of DPBF, and the degradation rate reached 56.68% at 90 min. The result might be contributed to that the pyridone structure in Py-Si could capture the $^1O_2$ produced by PpIX-Si to form endoperoxide for $^1O_2$ storage, and after removing the light source, the $^1O_2$ could still be continuously released under body temperature, indicating that Py-Si has the ability of rapid storage and sustained release of $^1O_2$ at 37 °C.

3.3. *Preparation and characterization of CTR-Py-PpIX*

PMMA polymer, an inexpensive, inert and well-tolerated intraocular implant material of CTR [28], was synthesized by polymerization reaction between MMA monomer, EGDMA crosslinker and AIBN initiator in this study. The obtained PMMA sheet was then processed into a bottom-opened CTR. However, as a surface hydrophobic material, PMMA is easily adhered by HLECs and proteins, resulting in the occurrence of PCO [28]. Reports showed that increase the roughness of PMMA via surface modification could inhibit the adhesion of cells and proteins [3,29]. Furthermore, PMMA is extremely chemically inert, making surface modification difficult. Therefore, to generate a large number of available active sites for chemical modification and inhibit cell proliferation and adhesion by altering the surface microstructure, a well-established solid surface treatment technology called inductively coupled plasma etching was applied to CRT surface modification. After treated by plasma etching system, the acquired CTR-O_2 plasma was immediately covalently conjugated with the photosensitizer unit PpIX-Si and the energy storage unit Py-Si via silanation reaction under the optimized molar ratio (PpIX-Si/Py-Si = 1/50) (Fig. 2A). To investigate the influence of feeding concentrations of PpIX-Si and Py-Si on the grafting degree in CTR surface, a series concentrations of PpIX-Si/Py-Si (0.01/0.5, 0.025/1.25, 0.08/4, 0.2/10, 0.5/25 mM) to prepare CTR-Py-PpIX were set, and the content of Si per surface area of CTR (ng/mm^2) of each group was determined. With the feeding concentration increased, the grafted amount of Si gradually increased, and tended to be saturated when the feeding concentration of PpIX-Si/Py-Si reached 0.2/10 mM (Fig. S5). Under the selected feeding concentration, the Si content per CTR surface area was detected to be 39.6 ng/mm^2.

The physical and chemical properties of CTR were shown in Fig. 2B and Table S1. The untreated CTR and CTR-O_2 plasma were colorless and transparent, after PpIX-Si and Py-Si grafting, the obtained CTR-Py-PpIX was light red, indicating the successful conjugation of PpIX-Si. Meanwhile, the macroscopic surface of the above CTR was smooth and uniform, with no obvious defects observed. The outer diameter of CTR-Py-PpIX was measured to be about 11.57 mm, and the variation deformation rate of the maximum diameter was about 0.17% when the compression reached 50% of deformation and released immediately, which is lower than 1% specified by the industry. The hardness of CTR, CTR-O_2 plasma and CTR-Py-PpIX measured by durometer were 1.05 ± 0.05 N, 1.04 ± 0.04 N, and 1.08 ± 0.04 N, respectively. The result suggested that the mechanical strength of CTR was nearly unchanged after plasma treatment and grafting (Table S1). After several times of extraction with 0.9% NaCl aqueous solution, the mass change of CTR was 0.22%, less than 0.5% specified by the industry, indicating an excellent quality stability of the CTR in aqueous humor. The above results revealed that the mechanical properties of CTR-Py-PpIX were good and basically meet the requirements of the industry.

The surface of CTR without plasma treatment is smooth without grooves in the SEM image, while a large number of grooves appeared on the surface of CTR-O_2 plasma (Fig. 2C), which not only enlarged the CTR surface area, but also provided abundant active hydroxyl groups for PpIX-Si and Py-Si conjugation. After covalently conjugated with PpIX-Si and Py-Si via silylation reaction, the surface groove structure of CTR-Py, CTR-PpIX and CTR-Py-PpIX maintained without

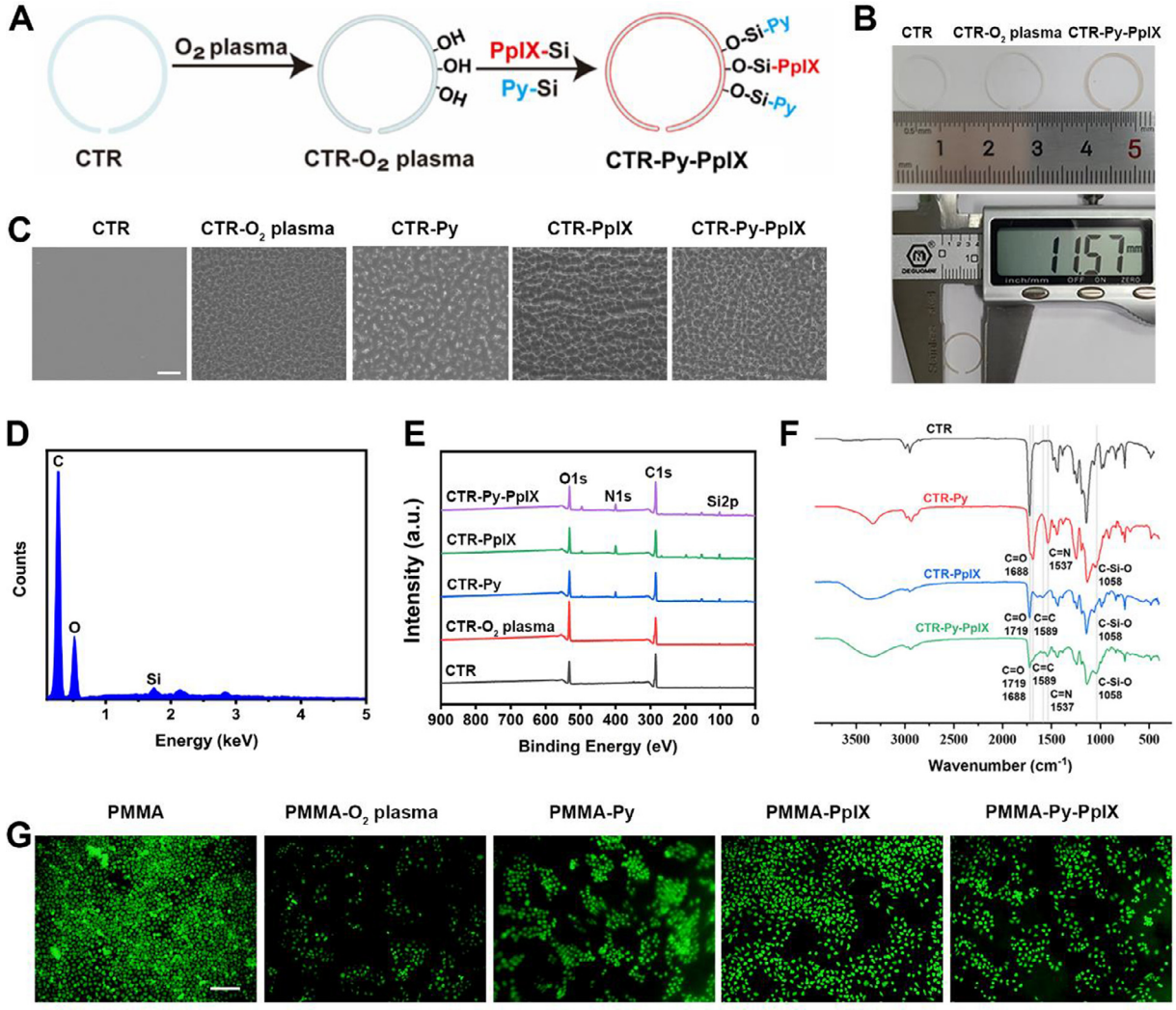

Fig. 2 – (A) Schematic illustration of CTR-Py-PpIX preparation. (B) The photograph of CTR, CTR-O_2 plasma and CTR-Py-PpIX. (C) The SEM image of CTR, CTR-O_2 plasma, CTR-Py, CTR-PpIX and CTR-Py-PpIX (Scale bar 20 μm). (D) The SEM-EDS spectrum of CTR-Py-PpIX. (E) XPS survery sepctrum of different CTR formulations. (F) FTIR spectrum of CTR, CTR-Py, CTR-PpIX and CTR-Py-PpIX. (G) The representative images of adhesion and proliferation of HLECs on different PMMA formulations (Scale bar 200 μm).

significant change, indicating the successful microstructure modification. To further verify the successful modification, the SEM-EDS and XPS analyses of the surface element composition were performed. The characteristic peak of Si appeared in the SEM-EDS spectrum (Fig. 2D). The XPS surveys of CTR and CTR-O_2 plasma displayed the principal spectra of O1s and C1s peaks centered at 531.93 ev and 284.78 ev, respectively. The O1s content of CTR-O_2 plasma (31.9%) was significantly higher than CTR (21.4%), while the C1s content decreased from 74.7% to 62.2%, indicating that hydroxyl group was introduced on the surface of CTR after O_2 plasma treatment. After Py-Si or PpIX-Si conjugation, new peaks attributed to N1s and Si2p centered at 399.83 ev and 102.33 ev were found in CTR-Py, CTR-PpIX and CTR-Py-PpIX (Fig. 2E). Since N element and Si element were appeared in Py-Si and PpIX-Si, these results suggested the successful conjugation of functional monomers.

FTIR was further conducted to verify the successful modification of Py-Si and PpIX-Si. Compared with CTR-Py, CTR-Py-PpIX contained the characteristic peaks at 1688 cm^{-1} and 1537 cm^{-1}, which assigned to the stretching vibration of C = O in amido bond and C = N bond, respectively (Fig. 2F). The result indicated the successful conjugation of Py-Si monomer on CTR-Py-PpIX. Compared with CTR-PpIX, CTR-Py-PpIX appeared the same characteristic peaks at 1719 cm^{-1} and 1589 cm^{-1}, which attributed to the stretching vibration of C = O in amido bond and C = C bond respectively, suggesting that PpIX-Si monomer had been grafted on the surface of CTR-Py-PpIX. Besides, compared with the untreated CTR, in addition to the characteristic peaks analyzed above, the stretching vibration peaks of C-Si-O at 1058 cm^{-1} appeared in CTR-Py, CTR-PpIX and CTR-Py-PpIX, indicating that PpIX-Si and Py-Si were successfully grafted on the surface of the CRT.

Since the surface microstructure of CTR was changed, as evidenced in the SEM image, the water contact angle of PMMA sheets after different treatments were detected and illustrated in Table S2. The contact angles of different groups ranked from low to high were PMMA-O_2 plasma < PMMA-Py < PMMA-Py-PpIX < PMMA-PpIX < PMMA. The maximum contact angle of the untreated PMMA group was 90.1° ± 22.0°, indicating the strongest surface hydrophobicity. The contact angle of PMMA-O_2 plasma group was significantly reduced to 27.8° ± 19.8°, indicating that the surface hydrophilicity was remarkably enhanced, possibly due to the generation of hydrophilic hydroxyl groups on the PMMA surface after plasma treatment. The hydrophilicity of PMMA-Py-PpIX group was between PMMA-Py and PMMA-PpIX and was similar to that of PMMA-Py, indicating that both Py-Si and PpIX-Si have been successfully grafted and the conjugated amount of Py-Si was more than that of PpIX-Si. The enhanced hydrophilicity of PMMA with plasma treatment facilitated its capacity to inhibit the migration and proliferation of LECs *in vivo*.

3.4. *Anti-cell adhesion and proliferation assay*

Since the microscopic groove structure and the hydrophilicity of CTR was increased after treated by plasma, next, whether the increase of roughness and hydrophilicity of PMMA could inhibit the adhesion of HLECs cells on PMMA-Py-PpIX surface was evaluated. The result of anti-cell adhesion and proliferation showed similar trend to water contact angle detection (Fig. 2G). The untreated PMMA group showed large amount of HLECs proliferated on its surface, which might be due to its smooth surface and certain hydrophobic properties. In sharp contrast, the PMMA-O_2 plasma group showed significantly reduced HLECs proliferation, which might be contributed to the increased surface roughness and hydrophilicity after plasma treatment. Compared with PMMA-Py and PMMA-PpIX groups, PMMA-Py-PpIX group displayed a moderate amount of green fluorescence, and the cells did not grow in large areas, indicating that after PpIX-Si and Py-Si grafting, the hydrophobicity of PMMA recovered to a certain extent. However, compared with the untreated PMMA, PMMA-Py-PpIX still had an excellent capacity to inhibit cell adhesion and proliferation (Fig. 2G).

3.5. *NIR triggered $^1O_2$ capture and release capacity of CTR-Py-PpIX*

The $^1O_2$ generation of CTR-Py-PpIX under NIR irradiation was determined using SOSG as a water-soluble $^1O_2$ indicator. SOSG with little fluorescent can selectively react with $^1O_2$ to form an internal SOSG endoperoxides (SOSG-EP) with prominent green fluorescence [30]. As shown in Fig. 3A, the fluorescence intensities of the control group and the CTR-Py group were nearly unchanged during the three-illumination cycle, indicating that SOSG and CTR-Py cannot generate $^1O_2$ under irradiation. In comparison, the fluorescence intensity of the CTR-PpIX group increased rapidly after the first 5 min of illumination and then remained unchanged when the irradiation was removed. Similar results were observed in the second and third irradiation cycle. The result indicated that CTR-PpIX could generate instantaneous $^1O_2$ during the PDT process, but it immediately stopped after stopping irradiation, possibly due to the short half-life and diffusion distance of $^1O_2$, which laid a solid foundation to serve as a $^1O_2$ donor. In sharp contrast, the fluorescence intensity of CTR-Py-PpIX group increased significantly after the first 5 min of irradiation, and it was continuously increased with time after stopping irradiation, and similar results were observed in the second and third irradiation cycle. These results suggested that Py has good $^1O_2$ storage and sustained release ability, realizing an instantaneously triggered sustainable PDT effect, which provided the possibility to continuously kill LECs after the CTR was implanted and illuminated by NIR.

3.6. *In vitro stability of CTR-Py-PpIX*

The chemical stability of CTR-Py-PpIX was investigated by detecting the content of Si released after immersed in artificial tears for different times. Negligible Si was detected at all the detected time points (Fig. 3B), indicating that Py-Si and PpIX-Si was stably conjugated on the surface of CTR without breakage, which effectively avoided the shedding of surface molecules to block the schlemm's canal, guaranteeing the safety of CTR-Py-PpIX when implanted in the eye. Next, the functional stability of CTR-Py-PpIX was further investigated. The CTR-Py-PpIX shaken in artificial tears for 1 and 16 d were taken out, and their NIR-triggered $^1O_2$ storage and release capacity were detected. The Day 1 CTR-Py-PpIX and Day 16 CTR-Py-PpIX maintained the similar capacity to generate and continuously release $^1O_2$ after removing the light source, as evidenced by the continuously increased fluorescence intensity during the three pre-NIR illumination cycle in the simulated aqueous circulating fluid (Fig. 3C and 3D). These results indicated the good PDT stability and $^1O_2$ storage and release stability of CTR-Py-PpIX, providing a guarantee for continuous LECs killing after the CTR was implanted in the eye. The above results revealed that CTR-Py-PpIX could stay stable in artificial tears for at least 16 d, with its PDT and $^1O_2$ storage and release functions maintained nearly unchanged, laying a strong foundation for sustainable intraocular therapeutic effect.

3.7. *In vitro cytotoxicity of CTR-Py-PpIX*

Live/dead cell staining assay was applied to intuitively observe the localized cell-killing effect of CTR using FDA/PI co-staining buffer. FDA and PI can stain live and dead cells to emit green and red fluorescence, respectively. Firstly, the cytotoxicity of CTR without $^1O_2$ storage (PDT effect) was evaluated on HLECs. Large amount of live cells (green fluorescence) and negligible dead cells (red fluorescence) were observed in control, CTR and CTR-Py groups, indicating that low-power (100 mW/cm²) and short-time (5 min) irradiation and CTR-Py had no cytotoxic effect on HLECs (Fig. 4A-4B). Moreover, CTR-Py-PpIX group without light irradiation also displayed little dead cells, indicating it had no dark toxicity. The CTR-PpIX (LS) group irradiated with 100 mW/cm² light for 5 min induced 75.5% of dead cells under the area covered by CTR, while extended the irradiation time to 10 min (CTR-PpIX (LL)) or increased the laser power to 200 mW/cm² (CTR-PpIX (HS)), 91.1% or 95% of dead cells were induced, respectively. By contrast, CTR-Py-PpIX group induced 95.1% of dead cells

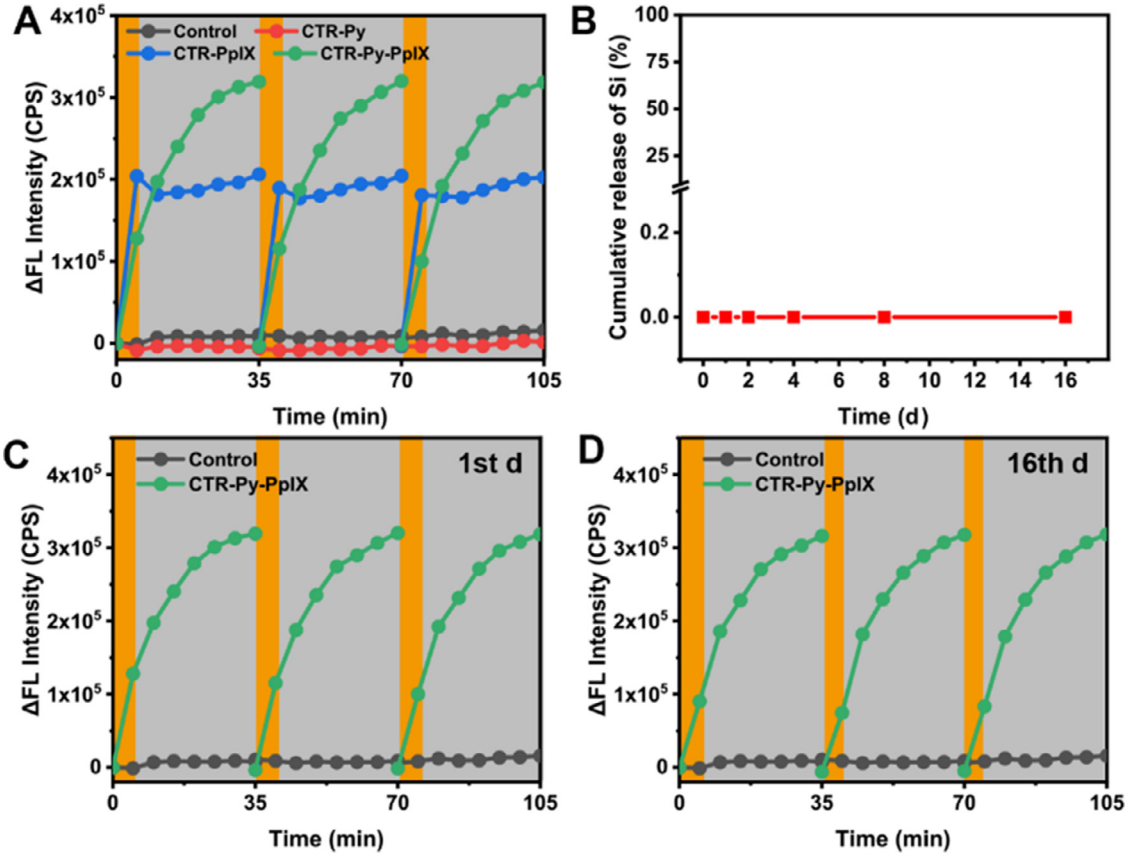

Fig. 3 – (A) Time-dependent curve of SOSG fluorescence intensity change of different surface modified CTR (The orange background represents NIR irradiation and the gray background represents dark placement). (B) The measurement of Si released from CTR-Py-PpIX by ICP-AES. $^1O_2$ capture and release capacity of CTR-Py-PpIX after shaken in artificial tears for (C) 1 d and (D) 16 d.

under short-term irradiation with low-power, indicating that CTR-Py-PpIX had high-efficient cell-killing effect under short-time irradiation and low laser power. The result might be because CTR-PpIX only possessed PDT effect that produce $^1O_2$ to kill cells, and the excess $^1O_2$ that had no time to damage cells quickly fails, while the $^1O_2$ generated by CTR-Py-PpIX could partially kill cells through PDT effect, and the other part immediately stored in Py, which further continuously released to kill cells after the cessation of PDT, enabling CTR-Py-PpIX to achieve better therapeutic effects even under low-power and short-time irradiation.

Next, the cytotoxicity of CTR with $^1O_2$ storage (battery effect) was investigated on HLECs. CTR, CTR-Py, CTR-PpIX and CTR-Py-PpIX which pre-illuminated with 630 nm laser (100 mW/cm²) for 5 min were immediately covered on the cell surface and incubated for 3 h prior to live/dead cell staining. As shown in Fig. 4C-4D, HLECs covered by the pre-illuminated CTR and CTR-Py displayed negligible dead cells, indicating that both CTR and Py had no cytotoxicity. CTR-PpIX group exhibited similar results to the control group, which might be attributed to the short half-life and diffusion distance of $^1O_2$ generated by PpIX-mediated PDT, which stopped immediately after removal of light irradiation. Intriguingly, both live and dead cells appeared in the CTR-Py-PpIX group under the coverage area, and the dead cells were accounted for about 21.3%, indicating that CTR-Py-PpIX could still release $^1O_2$ to induce cell-killing even after the irradiation was removed. The result might be due to that the $^1O_2$ produced during PDT was stored in Py-Si monomer and then continuously released after PDT was stopped, enabling the continuous oxidative treatment to enhance therapeutic effect. These results were consistent with the $^1O_2$ capture and release detecting experiment *in vitro*. The dual function of PDT and battery effect of CTR-Py-PpIX, as well as the characteristic of localized cell-killing in the contact area, provided a guarantee for high-efficient HLECs killing without damaging the surrounding retina and retinal nerve cells.

3.8. *Intracellular ROS and LPO levels detection*

3.8.1. *Intracellular ROS levels detection*

As the primary mechanism of PDT is induced by the production of $^1O_2$, one kind of highly cytotoxic ROS, the intracellular ROS levels was detected to investigate the cell-killing mechanism using DCFH-DA as a detecting indicator. DCFH-DA, a non-fluorescent molecular, can be hydrolyzed by intracellular esterase and further oxidized by intracellular ROS to emit green fluorescence [15,31]. Firstly, the intracellular ROS generation of CTR without $^1O_2$ storage (PDT effect) was detected. No obvious DCF green fluorescence

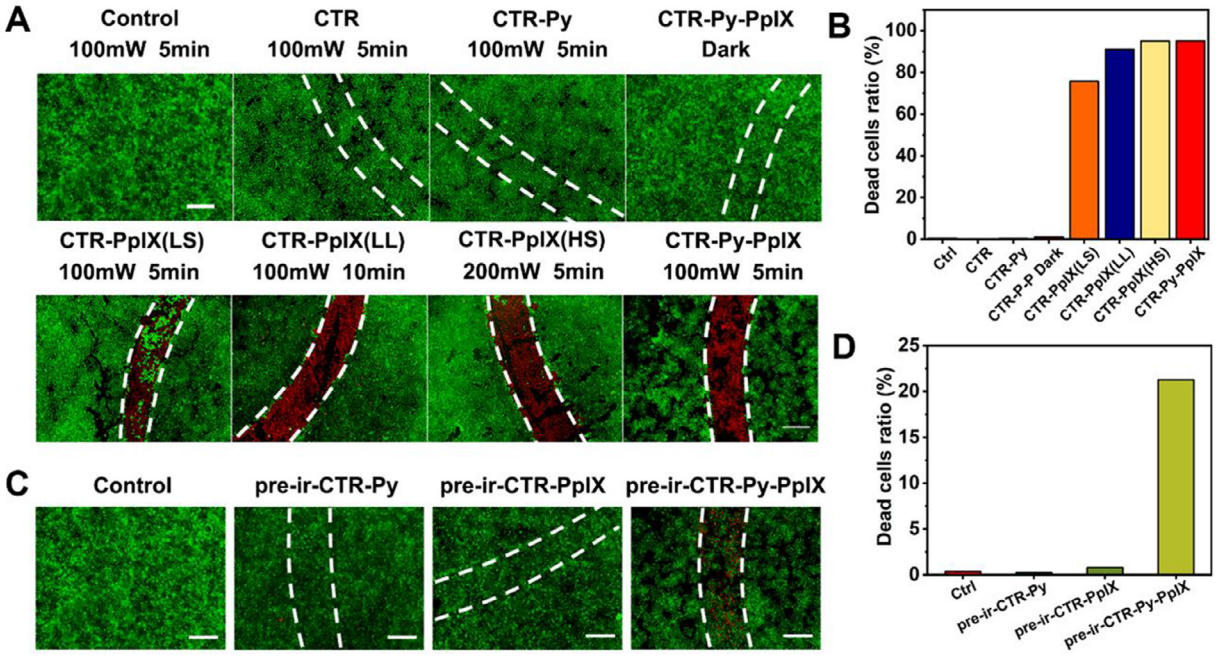

Fig. 4 – (A) The live/dead staining assay and (B) quantitative analysis of dead cells ratio (%) of HLECs treated with different CTR formulations and irradiation conditions for 3 h (Scale bar 500 μm). (C) The live/dead staining assay and (D) quantitative analysis of dead cells ratio (%) of HLECs treated with different pre-irradiated (630 nm, 100 mW/cm^2, 5 min) CTR formulations for 3 h (Scale bar 500 μm).

appeared in CTR and CTR-Py groups, indicating negligible ROS generation (Fig. 5A). Unexpectedly, CTR-PpIX and CTR-Py-PpIX with photosensitizer modification exhibited little green fluorescence as well, while free PpIX-Si group (positive control) displayed obvious green fluorescence, indicating that PpIX-Si could generate ROS intracellular. The undetectable ROS in CTR-PpIX and CTR-Py-PpIX groups might be caused by that the CTR was located extracellularly to perform PDT, the generated $^1O_2$ cannot enter the cell due to the extremely short half-life and diffusion distance. However, when free PpIX-Si was directly incubated with cells, the produced ROS could be detected intracellularly since PpIX-Si could enter into cells. Therefore, we speculated that the ROS-induced cell-killing effect of CTR-PpIX and CTR-Py-PpIX might originate from the damage of the cell membrane.

To further investigate the intracellular ROS generation of CTR with $^1O_2$ storage (battery effect), various pre-irradiated CTR groups were immediately covered on the surface of the DCFH-DA-treated cells. Neither the CTR, CTR-PpIX and CTR-Py groups nor the CTR-Py-PpIX group observed obvious ROS generation (Fig. 5B). However, the pre-irradiated free PpIX-Si + Py-Si group (positive control) displayed significant ROS production, indicating that PpIX-Si could generate ROS, which then stored in Py-Si to release $^1O_2$ intracellular. The undetected ROS in CTR-Py-PpIX group might be contributed to that the stored $^1O_2$ that released extracellularly cannot enter into the cells, further confirming that the cell-killing effect of the CRT preparations was not caused by the increase of intracellular ROS.

To further uncover whether the undetected intracellular ROS was caused by the extremely short half-life and diffusion distance of $^1O_2$ generated by CTR-Py-PpIX extracellularly, the ROS generation of free PpIX-Si and Py-Si that can enter into cells was evaluated. No obvious ROS was detected in Py-Si group, indicating that Py-Si was unable to generate ROS. Meanwhile, similar result was also observed in the pre-irradiated PpIX-Si group (Fig. 5C). In sharp contrast, pre-irradiated free PpIX-Si + Py-Si mixture group exhibited obvious ROS, and with the prolongation of incubation time, the amount of ROS in HLECs cells gradually increased (Fig. 5D). The result suggested that Py-Si could react with $^1O_2$ generated by PpIX-Si to generate Py-endoperoxide-Si, which could store $^1O_2$ in the form of chemical energy and prolong the half-life of $^1O_2$. After entering the cells, $^1O_2$ can be continuously released, resulting in the increase of intracellular ROS, and achieving the continuous PDT effect without further irradiation.

The above intracellular ROS detection results demonstrated that the pre-irradiated free PpIX-Si + Py-Si mixture group that could enter into cells increased the intracellular ROS levels, while the ROS generated by CTR-Py-PpIX was undetected intracellularly due to the extremely short half-life and diffusion distance. Thus, we assumed that the ROS-induced cell-killing effect of CTR-Py-PpIX might be caused by the damage of cell membrane, such as typically LPO reaction.

3.8.2. *Intracellular LPO levels detection*

To explore the specific performance of the extracellularly produced ROS to kill HLECs, intracellular LPO levels was detected using Bodipy C11 as a detecting indicator [16,32]. The stronger the green fluorescence is, the higher LPO levels are. The CTR light and CTR-Py light group observed negligible

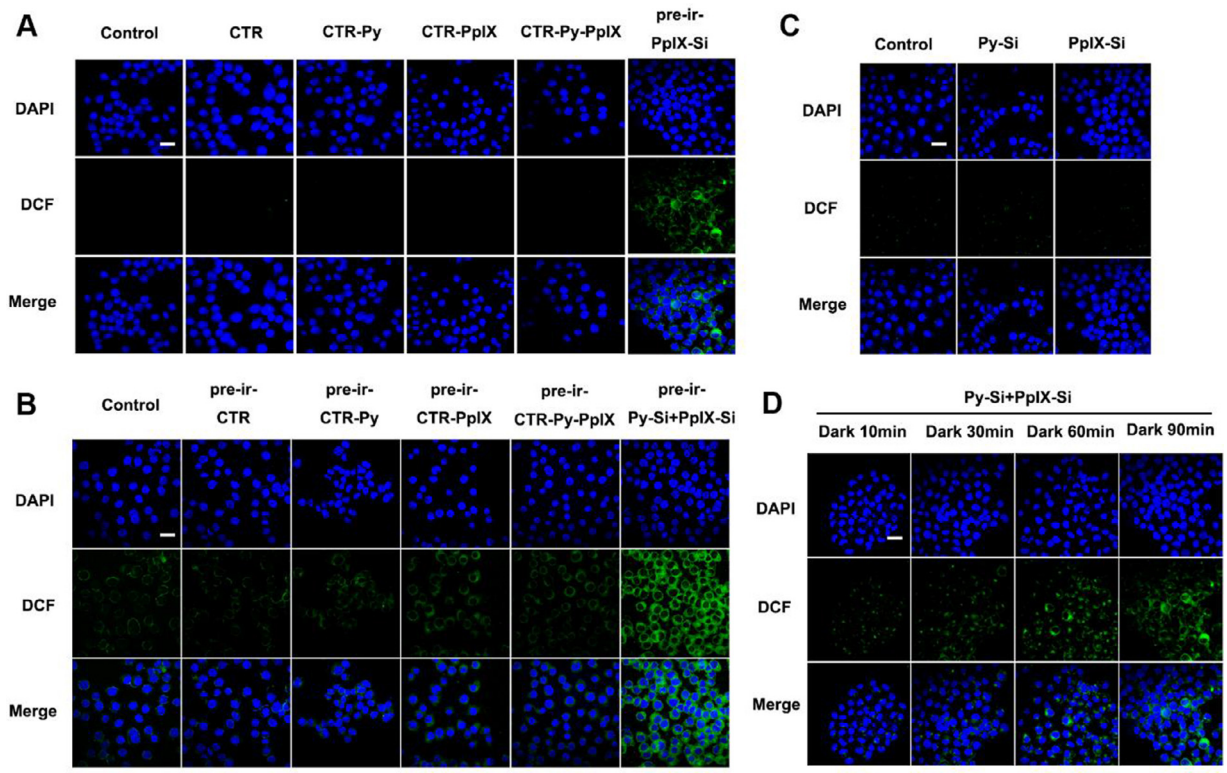

Fig. 5 – (A) The ROS generation of different CTR formulations that covered on HLECs with directly irradiation. (B) The ROS generation of different pre-irradiated CTR formulations that covered on HLECs. (C-D) The ROS generation of HLECs incubated with pre-irradiated free monomers. Irradiation condition: 630 nm, 100 mW/cm^2, 5 min. Scale bar 30 μm.

green fluorescence, indicating direct contact between CTR and the cells cannot induce LPO (Fig. 6A). The CTR-PpIX light group and the CTR-Py-PpIX light group induced moderate LPO levels under irradiation, possible due to the $^1O_2$ generation during the PDT process. Meanwhile, after the irradiation was stopped and continuously incubated under dark, the LPO levels of the CTR-PpIX light + dark group was similar to the CTR-PpIX light group, indicating that the $^1O_2$ production was highly synchronized with PDT, and the stop of irradiation means the stop of PDT. However, the LPO levels of the CTR-Py-PpIX light + dark group was significantly enhanced compared with the CTR-PpIX light + dark group, indicating that the irradiated CTR-Py-PpIX could still release $^1O_2$ after the illumination was removed, possibly because part of the $^1O_2$ was immediately stored by Py and then continuously released to aggravate the degree of LPO in the cell membrane, realizing long-lasting PDT effect.

To confirm that CTR-Py-PpIX could still release ROS after the light source was removed to aggravate the LPO levels in the cell membrane (battery effect), various pre-irradiated CTR groups were immediately covered on the surface of the Bodipy-C11-treated HLECs cells. Compared with the control group, the CTR, CTR-PpIX and CTR-Py groups observed negligible LPO generation, while the pre-irradiated CTR-Py-PpIX group induced significant LPO levels, and with the extension of incubation time, the levels of LPO in HLECs cells gradually increased (Fig. 6B). The result verified that the irradiated CTR-Py-PpIX could continuously release $^1O_2$ to exacerbate LPO levels after removing of illumination, enabling long-lasting PDT therapeutic effect.

Since cells have intracellular antioxidant system, LPO can be repaired when their levels are low. However, when oxidative stimuli are continuously given beyond the range of self-repair, the cell membrane will be irreversibly damaged, manifested as decreased cell membrane fluidity, increased fragility, or even ruptured to release the contents, eventually leading to cell death. Combined with the experimental results of live/dead cell staining, CTR-Py-PpIX had a stronger killing effect under low-power and short-time light conditions, which might be mainly due to the continuous release of $^1O_2$ to aggravate LPO levels, eventually leading to significantly enhanced cell membrane destruction and cell death.

3.9. *Pharmacodynamics investigation in the isolated lens capsular bag*

Inspired by the excellent cell-killing effect *in vitro*, the pharmacodynamics of CTR-Py-PpIX in the isolated lens capsular bag was further investigated to intuitively and truly evaluate the *in vivo* therapeutic effect. As shown in Fig. 7, the freshly isolated rabbit lens capsular bag was smooth and transparent on Day 0 under a digital inverted microscope, with a small amount of lens cortex remaining and almost no cell adhesion. After 1 d of incubation, the adhesion and proliferation of LECs appeared in the control, the CTR and the CTR-Py groups. With the incubation time increased, the LECs

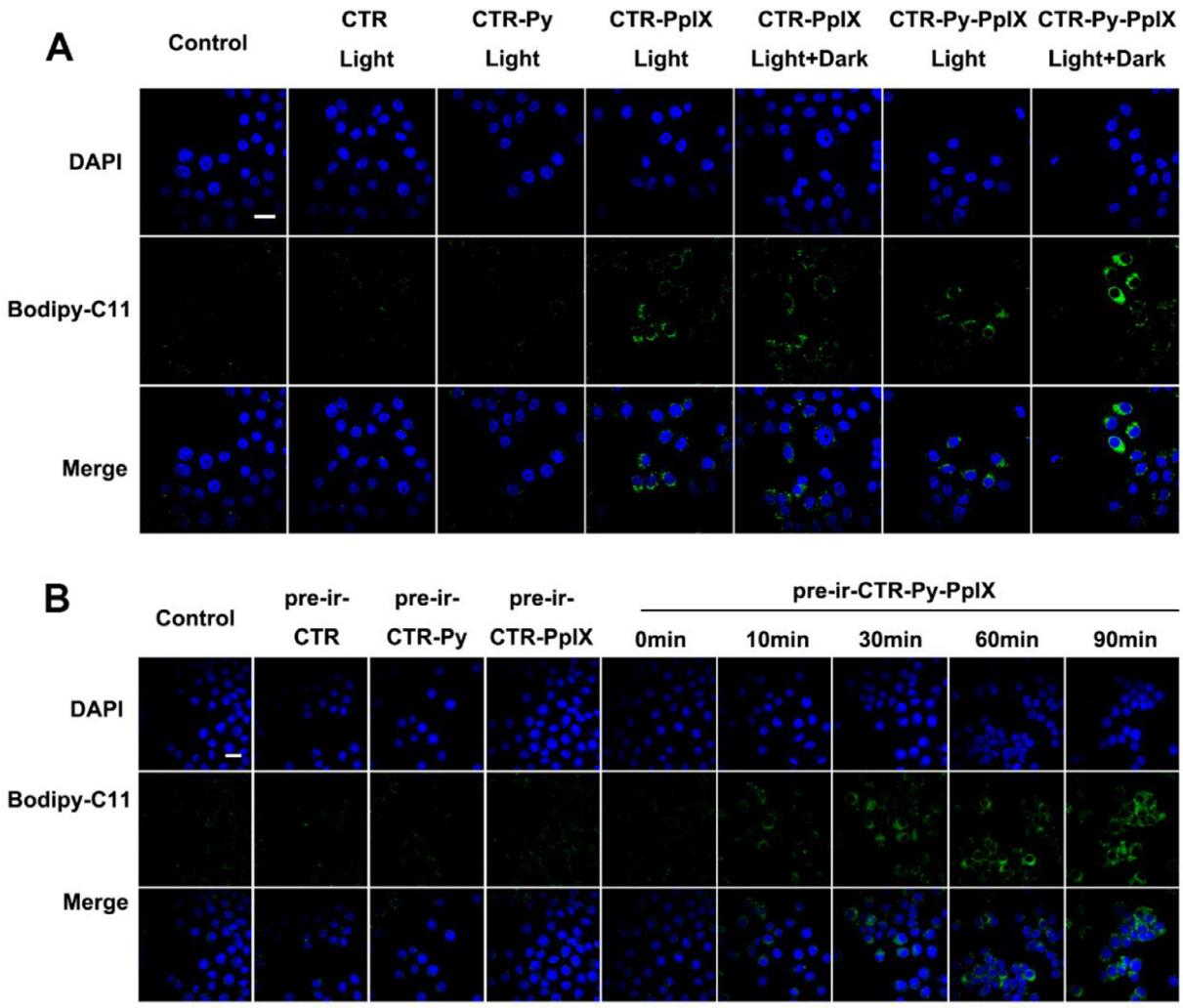

Fig. 6 – (A) The LPO levels of HLECs treated with different CTR formulations with directly irradiation. (B) The LPO levels of HLECs treated with different pre-irradiated CTR formulations. Irradiation condition: 630 nm, 100 mW/cm^2, 5 min. Scale bar 30 μm.

on the posterior capsule proliferated rapidly, and the capsular bag was covered by a large number of LECs at Day 3. Moreover, the posterior capsule was almost completely covered by LECs, and many spindle cells appeared at Day 5 and the cells are very closely arranged and even grow in clusters at Day 7, indicating that epithelial cells have undergone epithelial-mesenchymal transition. The result indicated that CTR and Py had little effect on inhibiting PCO. By contrast, the CTR-PpIX(LS) group (100 mW/cm^2, 5 min) displayed a slight cell residues with low power and short-time irradiation at Day 1, while increasing the laser power to 200 mW/cm^2 (CTR-PpIX (HS), 5 min) or extended the irradiation time to 10 min (CTR-PpIX (LL), 100 mW/cm^2), no obvious cell proliferation was observed. The proliferated cells remained in the CTR-PpIX (LS) group at Day 3 of incubation, and it was gradually proliferated with incubation time increased, with vigorous cell proliferation and numerous spindle cells appeared at Day 7. However, there was still obvious proliferated cells in the lens capsular bag in the CTR-PpIX (HS) and the CTR-PpIX (LL) groups even after 7 d of incubation. The results indicated that PDT-induced by CTR-PpIX was difficult to inhibit the adhesion and proliferation of LECs under low power and short time irradiation, but achieving significantly enhanced killing effect when increasing the light power or prolonging the irradiation time. Intriguingly, the CTR-Py-PpIX group (100 mW/cm^2, 5 min) could almost completely kill LECs cells under low power and short time irradiation, with no cell adhesion and proliferation observed at 7 d of incubation and the isolated capsular bag remained smooth and clean, indicating that short-term PDT combined with long-term continuous oxidative stimulation could also achieve good cell-killing effect.

The above results suggested that in the early stage of cell growth and proliferation after cataract surgery, completely inhibiting the remaining cells is of great significance to prevent and control the occurrence of PCO. Importantly, the application of low power and short-term illumination is critical for the protection of retinal cells and nerves. In addition, though the modified CTR had improved surface hydrophilicity and roughness to inhibit cell adhesion and proliferation *in vitro*, they showed ignorable effect in *ex-*

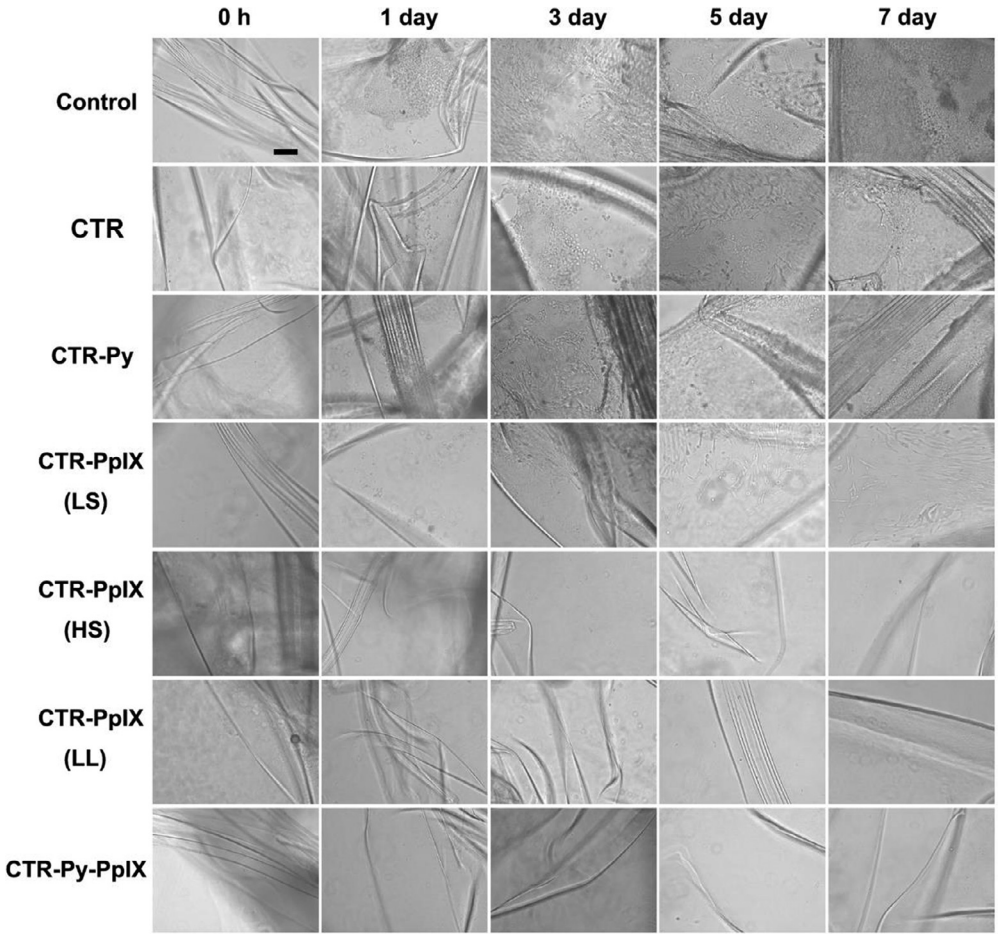

Fig. 7 – Growth status of LECs in lens capsule bag within 168 h after various treatments (Scale bar 200 μm).

vivo, but at least they wouldn't promote cell adhesion and proliferation. Reports showed that under the focusing function of the eye lens, the laser will be concentrated into a very small spot on the retina, and the retinal photoreceptor cells can be destroyed by an instantaneous increase of 10 °C [33]. At the same time, the eye will focus the NIR light on the retina. If the laser power is too high or the illumination time is too long, the laser beam focused on the retina will cause permanent damage in a very short time. When the localized retinal burst damage occurs, it will immediately form a permanent blind spot. In this case, the penetration of high laser power and prolonged exposure time can cause the retina to heat up, causing burns and even blindness. Therefore, the CTR-Py-PpIX designed in this work would be a promising intraocular implant to effectively prevent the occurrence of PCO while protecting the retina and optic nerve undamaged.

3.10. *Toxicity of CTR-Py-PpIX*

The biocompatibility of CTR-Py-PpIX was evaluated by observing the cell morphology and detecting the cell viability in L929 cells. The normal L929 cells were spindle-shaped and grow adherently to the wall (Fig. S6A). However, after phenol treatment, the cells shrunk into round shape and cell lysis occurred, and more than 50% of cell proliferation was inhibited. In sharp contrast, the L929 cells treated with the elution extracted from CTR-Py-PpIX exhibited similar cell morphology and growth state to the control group. The MTT results were consistent with morphology observations, with 100.15% and 0.64% cell viability detected in the elution group and phenol group, respectively (Fig. S6B). These results indicated that CTR-Py-PpIX had good biocompatibility and safety for further *in vivo* use.

4. Conclusions

In this study, a NIR-triggered ROS storage intraocular implant that concurrently functionalized with PDT generator PpIX and ROS reservoir Py was successfully developed. The as-designed CTR-Py-PpIX could ensure instantaneous ROS generation with irradiation and sustainable ROS production when removing irradiation, achieving a more efficient and safer long-term PDT for effective PCO prevention. The silylated PpIX-Si and Py-Si were covalently linked to the plasma activated CTR surface via silanization to obtain CTR-Py-PpIX, which guaranteed its long-term stability without drug leakage. The mechanical properties of CTR are good and nearly unchanged after modification, but the surface hydrophilicity

and roughness after plasma treatment increased for cell adhesion and proliferation inhibition. *In vitro* experiments revealed that CTR-Py-PpIX had dual functions of PDT and battery effect, which could generate ROS extracellularly under mild NIR conditions. With one part directly inhibiting LECs by LPO induction of cell membranes, the other part stored in Py continuously released to amplify LPO levels, ultimately realizing an sustainable and controlled PDT effect for continuous LECs killing. With instantaneous and sustainable ROS generation, the proliferation of LECs in ex-vivo capsule bag was completely inhibited with good biocompatibility. We believed that this NIR-triggered ROS storage CTR would be a promising intraocular implant for long-term PCO prevention.

Conflicts of interest

The authors declare no interest in this paper.

Acknowledgements

This work was financially supported by the National Natural Science Foundation of China (Grant number: 81973256/H3008, 82173748/H3408).

Supplementary materials

Supplementary material associated with this article can be found, in the online version, at doi:10.1016/j.ajps.2022.10.004.

REFERENCES

[1] Lei M, Peng Z, Dong Q, He Y, Zhang Z, Zhang X, et al. A novel capsular tension ring as local sustained-release carrier for preventing posterior capsule opacification. Biomaterials 2016;89:148–56.
[2] Awasthi N, Guo S, Wagner B. Posterior capsular opacification: a problem reduced but not yet eradicated. Arch Ophthalmol-Chic 2009;127(4):555–62.
[3] Xia J, Lu D, Han Y, Wang J, Hong Y, Zhao P, et al. Facile multifunctional IOL surface modification via poly (PEGMA-co-GMA) grafting for posterior capsular opacification inhibition. Rsc Adv 2021;11(17):9840–8.
[4] Zhang Z, Huang W, Lei M, He Y, Yan M, Zhang X, et al. Laser-triggered intraocular implant to induce photodynamic therapy for posterior capsule opacification prevention. Int J Pharmaceut 2016;498(1–2):1–11.
[5] Lin YX, Hu XF, Zhao Y, Gao YJ, Yang C, Qiao SL, et al. Photothermal ring integrated intraocular lens for high-efficient eye disease treatment. Adv Mater 2017;29(34):1701617.
[6] Cullin F, Busch T, Lundström M. Economic considerations related to choice of intraocular lens (IOL) and posterior capsule opacification frequency–a comparison of three different IOLs. Acta Ophthalmol 2014;92(2):179–83.
[7] Zhang X, Lai K, Li S, Wang J, Li J, Wang W, et al. Drug-eluting intraocular lens with sustained bromfenac release for conquering posterior capsular opacification. Bioact Mater 2022;9:343–57.
[8] Billotte C, Berdeaux G. Adverse clinical consequences of neodymium: YAG laser treatment of posterior capsule opacification. J Cataract Refr Surg 2004;30(10):2064–71.
[9] Huang X, Wang Y, Cai JP, Ma XY, Li Y, Cheng JW, et al. Sustained release of 5-fluorouracil from chitosan nanoparticles surface modified intra ocular lens to prevent posterior capsule opacification: an *in vitro* and *in vivo* study. J Ocul Pharmacol Th 2013;29(2):208–15.
[10] Xu JW, Li HN, Hu DF, Zhang XB, Wang W, Ji J, et al. Intraocular lens with mussel-inspired coating for preventing posterior capsule opacification via photothermal effect. Acs Applied Bio Mater 2021;4(4):3579–86.
[11] Weber CH, Cionni RJ. All about capsular tension rings. Curr Opin Ophthalmol 2015;26(1):10–15.
[12] Menapace R, Findl O, Georgopoulos M, Rainer G, Vass C, Schmetterer K. The capsular tension ring: designs, applications, and techniques. J Cataract Refr Surg 2000;26(6):898–912.
[13] Sun R, Gimbel HV. *In vitro* evaluation of the efficacy of the capsular tension ring for managing zonular dialysis in cataract surgery. SLACK Incorporated Thorofare 1998;29:502–5.
[14] Huang Y, Guan Z, Dai X, Shen Y, Wei Q, Ren L, et al. Engineered macrophages as near-infrared light activated drug vectors for chemo-photodynamic therapy of primary and bone metastatic breast cancer. Nat Commun 2021;12(1):1–22.
[15] Huang Y, Xiao Z, Guan Z, Shen Y, Jiang Y, Xu X, et al. A light-triggered self-reinforced nanoagent for targeted chemo-photodynamic therapy of breast cancer bone metastases via ER stress and mitochondria mediated apoptotic pathways. J Control Release 2020;319:119–34.
[16] Huang Y, Jiang Y, Xiao Z, Shen Y, Huang L, Xu X, et al. Three birds with one stone: a ferric pyrophosphate based nanoagent for synergetic NIR-triggered photo/chemodynamic therapy with glutathione depletion. Chem Eng J 2020;380:122369.
[17] Wang Q, Sun M, Li C, Li D, Yang Z, Jiang Q, et al. A computer-aided chem-photodynamic drugs self-delivery system for synergistically enhanced cancer therapy. Asian J Pharm Sci 2021;16(2):203–12.
[18] Li X, Lovell JF, Yoon J, Chen X. Clinical development and potential of photothermal and photodynamic therapies for cancer. Nat Rev Clin Oncol 2020;17(11):657–74.
[19] Zhou Z, Zhang L, Zhang Z, Liu Z. Advances in photosensitizer-related design for photodynamic therapy. Asian J Pharm Sci 2021;16(6):668–86.
[20] Huang Y, Lai H, Jiang J, Xu X, Zeng Z, Ren L, et al. pH-activatable oxidative stress amplifying dissolving microneedles for combined chemo-photodynamic therapy of Melanoma. Asian J Pharm Sci 2022;17(5):679–96.
[21] Kaiser PK, VIOCs Group. Verteporfin PDT for subfoveal occult CNV in AMD: two-year results of a randomized trial. Curr Med Res Opin 2009;25(8):1853–60.
[22] Tang J, Liu S, Han Y, Wang R, Xia J, Chen H, et al. Surface modification of intraocular lenses via photodynamic coating for safe and effective PCO prevention. J Mater Chem B 2021;9(6):1546–56.
[23] Weng XL, Liu JY. Strategies for maximizing photothermal conversion efficiency based on organic dyes. Drug Discov Today 2021;26(8):2045–52.
[24] Benz S, Nötzli S, Siegel JS, Eberli D, Jessen HJ. Controlled oxygen release from pyridone endoperoxides promotes cell survival under anoxic conditions. J Med Chem 2013;56(24):10171–82.
[25] Fudickar W, Linker T. Release of singlet oxygen from organic peroxides under mild conditions. ChemPhotoChem 2018;2(7):548–58.

[26] Huang L, Wei G, Sun X, Jiang Y, Huang Z, Huang Y, et al. A tumor-targeted Ganetespib-zinc phthalocyanine conjugate for synergistic chemo-photodynamic therapy. Eur J Med Chem 2018;151:294–303.
[27] Li X, Gao M, Xin K, Zhang L, Ding D, Kong D, et al. Singlet oxygen-responsive micelles for enhanced photodynamic therapy. J Control Release 2017;260:12–21.
[28] Wang B, Lin Q, Jin T, Shen C, Tang J, Han Y, et al. Surface modification of intraocular lenses with hyaluronic acid and lysozyme for the prevention of endophthalmitis and posterior capsule opacification. Rsc Adv 2015;5(5):3597–604.
[29] Chen Q, Yu S, Zhang D, Zhang W, Zhang H, Zou J, et al. Impact of antifouling PEG layer on the performance of functional peptides in regulating cell behaviors. J Am Chem Soc 2019;141(42):16772–80.
[30] Sharma SK, Hamblin MR. The use of fluorescent probes to detect ROS in photodynamic therapy. Reactive oxygen species. Springer; 2021. p. 215–29.
[31] Huang Z, Huang Y, Chen M, Chen J, Zeng Z, Xu X, et al. Bone-targeted oxidative stress nanoamplifier for synergetic chemo/chemodynamic therapy of bone metastases through increasing generation and reducing elimination of ROS. Chem Eng J 2020;399:125667.
[32] Ferrusola CO, Fernández LG, Morrell J, Sandoval CS, García BM, Rodriguez-Martinez H, et al. Lipid peroxidation, assessed with BODIPY-C11, increases after cryopreservation of stallion spermatozoa, is stallion-dependent and is related to apoptotic-like changes. Reproduction 2009;138(1):55–63.
[33] Chuang LH, Lai CC, Yang KJ, Chen TL, Ku WC. A traumatic macular hole secondary to a high-energy Nd: YAG laser. Slack Incorporated Thorofare 2001;32:73–6.